Modelling the residual mean meridional circulation at different stages of sudden stratospheric warming events

Andrey V. Koval[1,2], ~~Anna N. Bakhareva[1]~~Wen Chen[3], Ksenia A. Didenko[1,2], Tatiana S. Ermakova[1,2], Nikolai M. Gavrilov[1], Alexander I. Pogoreltsev[1,2], Olga N. Toptunova[1,2], Ke Wei[3], Anna N. Yarusova[1], Anton S. Zarubin[1]

[1]Atmospheric Physics Department, Saint-Petersburg State University, Saint-Petersburg, 198504, Russia
[2]Department of Meteorological Forecasts, Russian State Hydrometeorological University, Saint-Petersburg, Russia
[3]Center for Monsoon System Research, Institute of Atmospheric Physics, Chinese Academy of Sciences, Beijing, P. R. China-100029

Correspondence to: Andrey V. Koval (a.v.koval@spbu.ru)

Abstract. Ensemble simulation of the atmospheric general circulation at altitudes up to the lower thermosphere is performed using the 3-D nonlinear mechanistic numerical model MUAM. ~~Residual~~The residual mean meridional circulation (RMC), which is the superposition of the mean Eulerian and wave-induced eddy components, is calculated for the boreal winter. Changes in the vertical and meridional RMC velocity components are analyzed at different stages of simulated composite sudden stratospheric warming (SSW) event averaged over 19 model runs. The simulation results show a general decrease in RMC velocity components up to 30% during and after SSW in the mesosphere and lower thermosphere of the Northern Hemisphere. There are also increases in the downward and northward velocities at altitudes 20-50 km at the northern polar latitudes during SSW. Associated vertical transport and adiabatic heating can contribute to warming the stratosphere and downward shifting of the stratopause during the composite SSW. The residual mean and eddy mass fluxes are calculated for different SSW stages. It is shown that before the SSW, planetary wave activity creates wave-induced eddy circulation cells in the northern upper stratosphere, which are directed upwards at middle latitudes, northward at high latitudes and downwards near the North Pole. These cells increase heat transport and adiabatic heating in the polar region. During SSW, the region of upward eddy vertical velocity is shifted to high latitudes, but the velocity is still downward near the North Pole. After SSW, upward eddy-induced fluxes span to entire polar region producing upward transport and adiabatic cooling of the stratosphere providing the return of the stratopause to higher altitudes. Obtained statistically significant results on the evolution of RMC and eddy circulation at different SSW stages at altitudes up to the lower thermosphere can be useful for better understanding mechanisms of planetary wave impacts on the mean flow and for the diagnostics of the transport of conservative tracers in the atmosphere.

Keywords: residual circulation; wave-induced eddy circulation, sudden stratospheric warming; numerical modelling

1. Introduction

The main mechanism for the global transport of tracers ~~in~~between the troposphere and stratosphere is the meridional circulation (e.g., Dobson et al., 1929; Dobson, 1956; Brewer, 1949; Fishman and Crutzen, 1978), in which tropospheric air enters the stratosphere in the tropics, then travels to the poles and sinks down at middle and high latitudes of both hemispheres. At higher altitudes, it is essential to consider the meridional circulation producing mass transfer from the summer hemisphere to the winter one. In the last decades, there has been a surge of interest in the study of the atmospheric general circulation, which was mainly related to diagnostics of transport of atmospheric gas species and its forecasting (e.g., Butchart, 2014; Pawson et al., 2000; Gerber et al., 2012; Eyring et al., 2005; SPARC CCMVal, 2010). A large number of studies were also devoted to the analysis of meteorological reanalysis data and to the interpretation of observed atmospheric processes (e.g., Iwasaki et al., 2009; Sevior et al., 2012, etc.).

It is well known, that atmospheric planetary-scale waves can substantially modify the mean Eulerian meridional circulation, i.e. zonal averaging of the mean meridional and vertical flows is ineffective for analyzing the global transport of atmospheric species. In the momentum and energy equations, the wave fluxes of momentum and heat are partly compensated by advective momentum and heat fluxes (e.g., Charney and Drazin, 1961). With the Eulerian approach, similar compensation of wave and mean mass fluxes occurs also in the continuity equation. These features do not allow one to isolate the wave action from that of the mean flow. In order to overcome this disadvantage, it is essential to use alternative approaches to the analysis of the zonal-mean circulation, one of which is calculation of transformed Eulerian mean (TEM) circulation (e.g., Andrews and McIntyre, 1976) that is used in the present study. This approach provides effective diagnostics of wave impacts on the mean flow, and gives the ability to calculate the meridional transport of mass and tracers in the atmosphere. This method leads to the consideration of the so-called mean residual meridional circulation (RMC), which is a superposition of eddy-induced and advective zonal-mean flows. RMC estimates residual parts of the mean flow, which remain after partial compensation of the Eulerian zonal-mean circulation by the wave-induced eddy mass, momentum and heat fluxes (e.g., Shepherd, 2007). In its traditional form, the RMC is two-dimensional and formulas describing it include zonally averaged values of atmospheric parameters, (e.g., Holton, 2004).

Sudden stratospheric warming (SSW) events are among the most dramatic dynamical processes appearing at high latitudes of the middle atmosphere during winter. In the stratosphere during SSWs, the zonal-mean meridional thermal gradient (usually directed towards the equator in winter) reverses its direction to the opposite one. In the case of a major SSW, the eastward zonal velocity in the mid-latitude stratosphere also reverses, while in the case of a minor SSW, only a weakening of the zonal wind velocity is observed (e.g., Holton, 2004; McIntyre, 1982). SSW events can substantially affect the dynamics and energetics at different atmospheric layers (Siskind et al., 2010; Fuller-Rowell et al., 2010; Funke et al., 2010; Liu et al., 2011; Yuan et al., 2012; Sun and Robinson, 2009; Nath et al., 2016). Changes in the meridional circulation during different phases of SSW event have been recently studied by Tao et al. (2017), de la Camara et al. (2018) recently.). During SSW, the general circulation of the winter stratosphere undergoes significant changes, which, through wave interactions, can be transmitted to the upper atmosphere of both hemispheres.

Koval et al. (2019a) simulated the zonal mean Eulerian meridional circulation and its changes during SSW events. It was shown that the global-scale Eulerian mean meridional circulation in the middle atmosphere varies significantly at different stages of SSW, which is essential for the transport of mass and tracers in the middle and upper atmosphere. However, as stated above, the net transport of gas species should include contribution of wave-induced eddy fluxes and requires RMC calculating. In this study, we extend studies by Koval et al. (2019a) to calculate the RMC components based on the simulated wind and temperature fields for the boreal winter season. Changes in the RMC and eddy circulation during composite SSW events are studied up to the altitudes of the lower thermosphere using the atmospheric circulation model MUAM. Statistically significant ensemble results for altitudes up to the mesosphere and lower thermosphere (MLT) are obtained. The study of the RMC makes it also possible to calculate residual meridional mass fluxes and estimate changes in adiabatic heating/cooling rates at different SSW stages in the middle and upper atmosphere.

2. Methodology

In order to study the changes in the RMC at time intervals before, during and after simulated SSW events, the middle and upper atmosphere model (MUAM) is used to describe the general circulation at altitudes up to the lower thermosphere (Pogoreltsev et al., 2007). It is a 3-D nonlinear mechanistic numerical model. The horizontal grid steps of the model are 5.625° in longitude and 5° in latitude. The vertical grid has 48 nodes from the ground to 135 km along the log-isobaric coordinate $z = -H * ln (p/p_0)$, where p_0 is the surface pressure and $H = 7$ km is the pressure scale height. The MUAM is based on a standard set of primitive equations in the spherical coordinates used in the Cologne Model of the Middle Atmosphere – Leipzig Institute

for Meteorology (COMMA-LIM) described by Fröhlich et al. (2003). A detailed description of the MUAM and processes implemented into the model are presented by Gavrilov et al. (2005) and Pogoreltsev et al. (2007). Details of the numerical experiments and used methods for determining the dates of SSW onset are similar to those described by Koval et al. (2019a). According to the downward control principle, an important driving force of the atmospheric meridional circulation are planetary-scale waves and gravity waves (Haynes et al., 1991; Holton et al., 1995). The MUAM model reproduces spectra of global-scale and mesoscale wave disturbances (Pogoreltsev et al., 2014, Gavrilov et al., 2015; 2018) as well as atmospheric tides (Suvorova and Pogoreltsev, 2011). The amplitudes of stationary planetary waves (SPWs) at the lower boundary are calculated from the geopotential height distributions in the lower atmosphere obtained from reanalysis of meteorological information UK Met Office (Swinbank and O'Neill, 1994; Swinbank et al., 2004) and averaged over the years 1992-2011 for January. In addition, MUAM involves parameterization of westward travelling atmospheric normal modes (NMs) by adding terms to the heat balance equation in the troposphere, which have forms of time-dependent sinusoidal components with zonal wavenumbers m = 1 - 3. For setting the latitude structures of NM components, the parameterization uses respective Hough functions. Periods of NMs are equal to the resonant periods of atmospheric reaction to the wave forcing at ~~low~~lower boundary (Pogoreltsev et al., 2009). The model also includes parameterizations of the dynamic and thermal effects of stationary orographic gravity waves developed by Gavrilov and Koval (2013) and of nonorographic gravity waves (GWs). For the nonorographic GWs having phase speeds 5–30 m/s a parameterization based on the Lindzen's one (Lindzen, 1981) is applied. For the faster GWs (30–125 m/s) a version of the spectral parameterization (Yigit & Medvedev, 2009) is used. This parameterization uses 15 GW spectral components uniformly distributed within the period range from 40 min to 3 hr. Estimations by Pogoreltsev et al. (2007) and Gavrilov el al. (2015) showed that the MUAM satisfactorily reproduces the structure of atmospheric circulation up to altitudes of the lower thermosphere.

To improve the statistical significance and smooth out the interannual variability in the MUAM, an ensemble of 24 model runs was obtained and 19 runs containing stratospheric warming events for January-February were selected using the methodology described by Gavrilov et al. (2018). Different MUAM runs correspond to different phases of vacillations between the mean wind and SPWs in the middle atmosphere. These phases in the MUAM are controlled by changing the date of triggering daily variations in the solar heating and generation of normal atmospheric modes in different ensemble members of model runs (Pogoreltsev et al., 2007, 2009).

The onset dates of simulated SSWs were obtained using the definition by Charlton and Polvani (2007). However zonal wind reversals at every MUAM run were frequently detected not at pressure level of 10 hPa (near 30 km altitude), but at higher altitudes up to 50 km (Gavrilov et al., 2018). Savenkova et al. (2017) investigated SSWs using MERRA-2 reanalysis data (Gelaro et al., 2017) for the years 1980 – 2016. They showed that nearly half of the warmings were accompanied by a reversal of the zonal wind above 10 hPa pressure level. Such warmings cannot be treated as major SSWs according to the definition by the WMO, and the term "high stratospheric warmings" (HSWs) was introduced to denote them. Types of the reproduced SSW events may be different for different MUAM runs. A set of 19 simulated warming events contains 5 major SSWs, 7 HSWs and 7 minor SSWs.

Figure 1 shows examples of SSW events simulated with the MUAM for different phases of stratospheric vacillations. Shaded areas in the left and right panels are the zonal-mean temperature averaged over latitude band 82-87° N and the zonal-mean zonal wind, respectively. Zero time in Figure 1 corresponds to the onset day of simulated SSW. The panels a – d of Figure 1 correspond, respectively, to typical cases of major SSW, HSW, minor SSW and a MUAM run without stratospheric warming. An interesting feature of the left panels of Figure 1 is the downward shift of the stratopause during SSWs and its return to higher altitudes after simulated SSWs. This effect is more pronounced for stronger major SSW in the left panel of Figure 1a, where one can observe so called "elevated stratopause" after SSW. Similar behavior of the stratopause was obtained in simulations with the Whole Atmosphere Community Climate Model (Chandran et al., 2013). Another examples of temperature

and wind variations during SSW events simulated with the MUAM can be found in Figures 1 of the papers by Koval et al. (2019b) and Gavrilov et al. (2018).

125 In the present study, the onset date for each simulated SSW event was determined and three 11-day consecutive intervals were selected before, during and after the event. These intervals are indicated with horizontal lines above the panels in Fig. 1. After averaging over these intervals and over all simulated SSWs, this approach allowed us to obtain characteristics for a composite SSW event statistically relevant to the SSW climatology obtained by analyzing multi-year reanalysis data and described by Savenkova et al. (2017).

130 ### 3.   Calculating the residual mean meridional circulation

Residual circulation in this study is understood in the context of the transformed Eulerian mean approach (Andrews et al., 1987). The meridional and vertical components of the RMC within the TEM approach can be calculated by the formulas described by Andrews et al. (1987) and Butchart (2014):

$$\overline{v}^* = \overline{v} - \rho^{-1} \frac{\partial}{\partial z}\left(\rho \frac{\overline{v'\theta'}}{\partial \overline{\theta}/\partial z} \right), \tag{1}$$

135
$$\overline{w}^* = \overline{w} + \frac{1}{a\cos\varphi} \frac{\partial}{\partial \varphi}\left(\frac{\cos\varphi\,\overline{v'\theta'}}{\partial \overline{\theta}/\partial z} \right), \tag{2}$$

where the overbars denote the zonal-mean values, the dashes mark the deviations of hydrodynamic quantities from their zonal-mean values; $v' = v - \overline{v}$; $\theta' = \theta - \overline{\theta}$; v and w are the meridional and vertical components of wind; ρ is background atmospheric density; z is vertical log-isobaric coordinate; θ is potential temperature; φ is latitude; a is the Earth's radius. ~~Introducing deviations from the mean zonal components of the wind velocity and potential temperature as $v' = v - \overline{v}$; $\theta' = \theta - \overline{\theta}$ one~~

140 ~~can rewrite Eq.~~After some calculus one can rewrite Eq. (1) and (2) in the convenient form used in this study for calculating the meridional and vertical components of the residual mean circulation from the wind and temperature fields simulated with the MUAM:

$$\overline{v}^* = \overline{v} - \frac{1}{\partial \overline{\theta}/\partial z}\left(-\frac{\overline{v'\theta'}}{H} + \frac{\partial \overline{v'\theta'}}{\partial z} - \frac{\overline{v'\theta'}}{\partial \overline{\theta}/\partial z}\frac{\partial^2 \overline{\theta}}{\partial z^2} \right), \tag{3}$$

$$\overline{w}^* = \overline{w} + \frac{1}{a\cos\varphi}\frac{1}{\partial \overline{\theta}/\partial z}\left(-\sin\varphi\,\overline{v'\theta'} + \cos\varphi\left(\frac{\partial \overline{v'\theta'}}{\partial \varphi} - \frac{\overline{v'\theta'}}{\partial \overline{\theta}/\partial z}\frac{\partial^2 \overline{\theta}}{\partial z\partial \varphi} \right) \right). \tag{4}$$

145 In contrast to the zonal-mean Eulerian circulation (having velocity components $\overline{v}$ and $\overline{w}$) the residual vertical velocity $\overline{w}^*$ is proportional to the net rate of diabatic heating. It roughly represents a diabatic circulation in the meridional plane (Shepherd, 2007), i.e., when the heating of ascending air parcels and the cooling of descending air take place, while their potential temperature adapts to the local environment. Thus, the time-averaged RMC approximates the average movement of air masses and, therefore, it can be considered as transport of conservative atmospheric tracers.

150 Figure 2 shows a comparison of RMC ~~schematic streamlines and~~ wind vectors simulated with the MUAM (~~the top panels~~a) with those obtained from the database of meteorological reanalysis MERRA-2 (Gelaro et al., 2017) for the year 2010 (~~the bottom panels~~b). The ~~streamlines~~arrows in Figure ~~2a~~2 show two main RMC cells with an upwelling at low and middle latitudes of the Southern Hemisphere and downwelling at high latitudes of both hemispheres. The Eulerian mean meridional circulation in the troposphere and stratosphere should usually consist of tropical Hadley cells controlled by diabatic heating, eddy-induced

155 mid-latitude Ferrell cells and polar cells generated by temperature gradients (e.g., Holton, 2004). In contrast to that, the residual circulation should consist of two Hadley cells transporting air masses from low to high latitudes (Butchart, 2014), which are

visible in Figure 2. At the same time, in winter (Northern) Hemisphere, the circulation cell is much wider than that in the summer (Southern) Hemisphere with higher residual meridional and vertical velocities shown ~~with arrows~~ in Figure ~~2b~~2.

Comparisons of ~~the top~~Figures 2a and ~~bottom panels of Figure 2a~~2b show a correspondence between the structure of the simulated RMC and that obtained from the reanalysis data. ~~In~~Some differences in the ~~top and bottom panels of Figure 2b one can see magnitudes of RMC~~ wind vectors. ~~Some differences~~ in the upper troposphere can be connected with rather schematic representation of the tropospheric dynamics in the model. Birner and Bönisch (2011) calculated the RMC based on the data from the Canadian Middle Atmosphere Model and obtained streamline distributions for January, which ~~are similar to those~~reflect the RMC structure shown in Figure 2a. Eluszkevicz et al. (1996) analyzed the RMC using modelling and observations with the Microwave Limb Sounder onboard the Upper Atmosphere Research Satellite. They presented the distributions of the vertical and meridional wind components, which are consistent with our Figure ~~2b~~2a. The RMC structure shown in Figure 2 is also in agreement with that obtained by Gille et al. (1987) and Kobayashi and Iwasaki (2016). The latter study presents the RMC fields for winter in the Northern Hemisphere obtained with the data from the Limb Infrared Monitor of the Stratosphere on the Nimbus-7 satellite and from the JRA-55 reanalysis data (Kobayashi et al., 2015).

Studies of the evolution of hydrodynamic fields during SSW events have limitations due to relatively large time spacing of meteorological observations (several hours) and due to difficulties of estimating vertical velocity from meteorological data. Numerical modeling can help to overcome these difficulties. Also, usage of mechanistic numerical models enables one to perform series of model runs for the same climatological conditions to increase statistical confidence of obtained results. In addition, numeric modeling allows us to study RMC changes during SSW rectified from superimposing other extreme events, which could exist in experimental data.

4.   Residual circulation at the different SSW stages

In this section, we observe the changes in RMC at altitudes of 0 – 100 km during different stages of the composite SSW event (averaged over 19 model runs) simulated with the MUAM. Residual velocity components are calculated applying Eq. (3) and (4) to the wind and temperature fields obtained at each MUAM run. Then these characteristics are averaged over 19 model runs, separately, for 11-day intervals "before", "during" and "after" SSW (see section 2).

Figure 3a shows the distributions of the simulated with the MUAM residual meridional and vertical velocities averaged over 11-day intervals before the composite SSWs. Top and bottom panels of Figure 3a correspond to the main cells of the RMC, ~~which~~its general structure is presented in Figure 2. Also, RMC structure is consistent with the current knowledge (e.g., Tegtmeier et al., 2008). The main maximums of the residual meridional velocity in Figure ~~2a1~~3a1 exist at altitudes 40 – 50 km and 70 – 90 km. They form downward residual flows in the Northern Hemisphere and upward flows in the Southern Hemisphere in Figure 3a2, which contribute to the warming of the atmosphere near the North Pole and cooling near the South Pole in January due to adiabatic temperature changes inside vertically moving atmospheric parcels.

Figures 3b and 3c represent add-ons of the residual velocity components during and after the composite SSW relative to the distributions before the event in Figure 3a. The hypothesis of nonzero differences in Figures 3b and 3c was verified with the statistical paired Student's t-test (e.g., Rice, 2006). At each latitude-height grid point the data in Figures 3b and 3c is averaged over $66\times19 = 1254$ individual differences (11 days with 4-hour outputs for 19 model runs). The paired Student's t-test gave statistical confidence of nonzero differences larger 95% for almost all values shown in Figures 3b and 3c.

Figures 3b1 and 3b2 demonstrate signs of the add-ons to the residual velocity components, which are generally opposite to the signs of meridional and vertical residual velocities in Figures 3a1 and 3a2 and correspond to general RMC weakening (up to 30%) during the SSW. However, Figure 3b1 demonstrates positive add-ons to the residual meridional velocity at high northern latitudes at heights of 20 – 70 km. They increase transport of heat to the polar regions and form negative add-ons to the background downward vertical velocity at altitudes of 20 – 50 km and positive add-ons at altitudes ranging from 50 to 100 km

at high northern latitudes in Figure 3b2. ~~The~~In the Figure 1 the contours ~~at the left and right panels of Figures 1 indicate~~are shown indicating residual vertical and meridional velocities (in the left and right panels, respectively) at high northern latitudes for specific MUAM runs, which generally confirm discussed above behavior of average distributions shown in Figure 3b. During SSW, magnitudes of downward and upward residual vertical velocities near the North Pole can reach ~~|w*|~~ $|\overline{w}*|$ ~ 1 – 2 cm/s in Figure 1. Similar orders of ~~|w*|~~ $|\overline{w}*|$ magnitude during SSW were obtained for specific runs of the WACCM numerical model in Figure 1 of the paper by Chandran et al. (2013). Downward flows at altitudes of 20 – 60 km near the North Pole during SSW can move the warm stratopause down with the speed up to 1 – 2 km/day in Figure 3b2. In addition, vertical displacements of air parcels produce adiabatic heating/cooling, the specific rate of which is proportional to the residual vertical velocity (e.g., Gavrilov et al., 2020):

$$\cancel{\varepsilon_a = -\gamma_a w*; \quad \gamma_a = g/c_p,} \quad \varepsilon_a = -\gamma_a \overline{w}*; \quad \gamma_a = g/c_p, \tag{5}$$

where g is the acceleration due to gravity, c_p is the specific heat capacity of air at constant pressure, which corresponds to $|\varepsilon_a|$ ~ 10 – 20 K/day. During several days, such mechanism can provide heating up to several tens of degrees in the polar stratosphere at altitudes of 20 - 50 km in the region of negative ~~w*~~ $\overline{w}*$ in Figure 3b2 and comparable cooling in the region of positive ~~w*~~ $\overline{w}*$ at altitudes of 50 – 80 km. Such adiabatic cooling of the mesosphere and heating of the stratosphere can help to the downward shift of the stratopause during SSW, which can be seen in the left panels of Figure 1.

Figures 3c1 and 3c2 reveal that after SSW, add-ons of residual meridional and vertical velocity have signs generally opposite to the RMC before SSW in Figures 3a1 and 3a2, respectively. Similar weakening of the mean Eulerian global meridional circulation was shown in Figure 3 of the paper by Koval et al. (2019a). At polar northern latitudes below 50 km, the add-ons to the residual meridional velocity are directed to the South and the vertical velocity add-ons are strong and directed upwards. The region of the positive residual meridional velocity add-ons at altitudes of 60 – 70 km remains after SSW in Figure 3c1 and corresponds to downward add-ons to the vertical velocity at altitudes of 45 - 60 km in the northern polar region in Figure 3c2. Such behavior of RMC corresponds to evolutions of residual meridional and vertical components after SSW in Figure 1. In the northern polar region, strong upward ~~w*~~ $\overline{w}*$ below 40 - 50 km and strong downward ~~w*~~ $\overline{w}*$ above this layer create, respectively, fast upward transport and strong adiabatic cooling of the stratosphere and heating of the mesosphere restoring the ~~tropopause~~stratopause heights in Figure 1. Considerations of Figure 1 and similar figures from the paper by Chandran et al. (2013) allow us to conclude that downward winds above altitudes 40 – 50 may be stronger after major SSW. This may create increased heating of the mesosphere and upper stratosphere leading to effects of elevated polar stratopause after strong SSW (Chandran et al., 2013). An example of such increased heating at altitudes above 50 km one can see in the left panel of Figure 1a.

In the Southern Hemisphere, the main differences in RMC during and after simulated SSWs are demonstrated in Figures 3b and 3c at the MLT altitudes. These differences have signs generally opposite to the respective velocities shown in Figures 3a before SSWs. Absolute values of the differences at altitudes near 90 km are larger after SSW (Figure ~~3b1~~3c) than those during SSW (Figure ~~3b2~~3b). This determines weakening of the northward residual meridional velocity at altitudes 80 – 100 km in the mid-latitude Southern Hemisphere up to 25 – 30 % during the composite SSW and up to 30 – 40 % after SSW compared to that before the warming event in Figure 3a1. Respective decreases in the upward residual vertical velocity are demonstrated in Figures 3b2 and 3c2 at altitudes 80 – 100 km in the Southern Hemisphere. These changes may be produced by the inter-hemispheric coupling at the MLT heights caused by SPWs. These waves propagate upward from the troposphere through the circulation structures of the winter middle atmosphere (e.g., Charney and Drazin, 1961). Above the stratospheric heights, SPWs propagate along the waveguides, which span to both hemispheres at altitudes above 60 – 70 km (e.g., Koval et al., 2019b). Gavrilov et al. (2018) showed that in the stratosphere below 50 km, amplitudes of SPW1 with zonal wavenumber m = 1 are increased before simulated SSWs and decreased during the events, while changes in SPW2 amplitudes are opposite.

The modified SPWs in the northern stratosphere before and during SSW (Stray et al., 2015; Gavrilov et al., 2018) can then propagate along the waveguides to the southern upper atmosphere. Laskar et al. (2019) showed similar significant weakening (up to a reversal) of both the mean and residual meridional circulation at MLT heights during SSW observed in winters 2009/10 and 2012/13, causing temperature fluctuations in the stratosphere of both hemispheres. Larger velocity add-ons in the southern MLT region after SSW in Figure 3c compared to those during SSW in Figure 3b may reflect time delay for SPW propagation from the Northern to the Southern Hemisphere. In addition, simulated RMC velocity add-ons after SSWs could be partly produced by seasonal changes in the global circulation, as far as time intervals after SSW have 3-week time shift compared to respective intervals before SSW.

Recently, several studies have been devoted to the analysis of the peculiarities of the RMC formation and development during SSW events. Using data from the reanalysis of meteorological information, Song and Chun (2016) considered the contributions of various terms of the transformed Eulerian equations of temperature and angular momentum to the RMC formation at different SSW stages. Bal et al. (2017) studied the changes in the RMC based on the analysis of 76 model SSWs and of 17 major SSWs selected from the Era Interim reanalysis data. In both studies mentioned above, it was confirmed that large-scale wave disturbances are the main driving force of the RMC due to the transfer of energy and angular momentum in the middle atmosphere and the MLT region.

Increased downward residual vertical velocities at altitudes of 20 – 60 km at high northern latitudes during SSWs in Figure 3b1 correspond to the increased net downward mass flows and to increased adiabatic ~~cooling~~heating rate (5) in the heat balance equation of the model. This may help to heat the polar stratosphere. Therefore, changes in the RMC may influence the mechanisms of SSW formation at high latitudes.

5. Residual fluxes of mass.

RMC can create zonal-mean fluxes of mass in meridional plane, which can provide substantial global-scale transport of heat and conservative tracers in the atmosphere (e.g., Fishman and Crutzen, 1978). The meridional, F^*_x, and vertical, F^*_z, components of residual mass fluxes can be calculated by multiplying the atmospheric density by the residual meridional and vertical velocities, respectively, at each grid node as follows:

$$\cancel{F_i^* = \rho v_i^*, \qquad \rho = \frac{p_0}{RT}\exp\left(\int_0^h \frac{gdh}{RT}\right),} \quad F_i^* = \rho \overline{v}_i^*, \qquad \rho = \frac{p_0}{RT}\exp\left(-\int_0^h \frac{gdh}{RT}\right),$$

(6)

where $i = x, z$ correspond to meridional and vertical components, respectively; p_0 is pressure at the ground (at $h = 0$); R is the gas constant for dry air; T and h are temperature and geopotential height simulated with the MUAM at each grid node.

Arrows in Figure 3a2 show schematic vectors representing zonal-mean RMC mass flux (6) averaged over 11-day intervals before the composite SSW. In the stratosphere, these arrows correspond to RMC cells shown in Figure 3a and show tropical upwelling and extratropical downwelling with maximum meridional velocity at altitudes of 40 – 50 km of the winter hemisphere. At altitudes above 50 km, the RMC mass transport is directed from high latitudes of the summer hemisphere to high latitudes of the winter hemisphere having maximum meridional component at altitudes of 80 – 90 km in Figure 3a2. Both RMC cells produce downward mass fluxes at the middle and high latitudes of the winter hemisphere, which are maximized at altitudes 70 – 80 km near the North Pole in Figure 3a2 and can significantly influence thermal regime and transport of conservative tracers in the middle and high atmosphere.

Arrows in Figures 3b2 show add-ons ΔF^*_x and ΔF^*_z to the zonal-mean residual mass fluxes during simulated SSWs, which are averaged over 19 MUAM runs. Directions of arrows in Figure 3b2 are generally opposite to those in Figure 3a2 showing that RMS mass fluxes become generally smaller during simulated SSWs, which corresponds to the changes in RMC velocity

components shown with colors in Figure 3b. However, at altitudes 60 – 80 km at middle northern latitudes arrows in Figure 3b2 have the same directions as those in Figure 3a2 increasing northward mass fluxes during SSW. This increase in the RMC meridional component corresponds to negative ΔF^*_z at altitudes 20 – 50 km and positive ΔF^*_z at altitudes 50 – 70 km near the North Pole, which increase downward fluxes below 50 km and may form upward fluxes above 40 – 50 km during strong SSW at polar region as it is shown in Figure 1. As was discussed in the previous section, respective advection of heat and adiabatic heating below 50 km and cooling above may form downward shift of the stratopause during SSW (see Figure 1).

Arrows in Figures 3c2 show add-ons to the zonal-mean residual mass fluxes after simulated SSWs, which have directions generally opposite to the arrows in Figure 3a2 before SSW and denote weakening the global RMC mass transport. Near the North Pole, Figure 3c2 reveals positive ΔF^*_z at altitudes below 40 km and negative ΔF^*_z at altitude ranging from 40 to 60 km, which produce additional adiabatic cooling in the stratosphere and heating in the mesosphere helping to restore the stratopause height after SSW (see Figure 1 and section 4). After strong SSWs, downward mass fluxes above altitude of 40 km may intensify and respective adiabatic heating may help in forming effects of elevated stratopause (Chandran et al., 2013).

In the Southern Hemisphere, the main add-ons ΔF^*_x and ΔF^*_z in Figures 3b2 and 3c2 exist at altitudes above 70 km and are stronger after SSW. They have directions opposite to the mass fluxes of Figure 3a2, which corresponds to weakening of the global RMC. One of the reasons for these changes could be propagation of SPW from the Northern hemisphere along the waveguides crossing the equator at altitudes above 60 – 70 km (Gavrilov et al., 2018; Koval et al., 2019b).

Studies of the global transport of mass with RMC are important for estimating respective transport of conservative aerosol and gas species, which are responsible for the climate changes. One of such gases is ozone. Estimations of photochemical lifetime of atmospheric ozone (Jacob, 1999) give values longer than a month at altitudes lower than 30 km. Therefore, at low altitudes ozone fluxes may follow the RMC mass fluxes considered in this section. At higher altitudes, interactive models of atmospheric chemistry and dynamics are required for proper description of atmospheric ozone.

6. Wave-induced eddy circulation.

Differences between the residual and Eulerian zonal-mean velocity components ~~$v' = v^* - v_0$; $w` = w^* - w_0$~~ $v_{eddy} = \overline{v}^* - \overline{v}$; $w_{eddy} = \overline{w}^* - \overline{w}$ describe so-called eddy circulation, which give contributions of non-zonal motions produced mainly by planetary waves (Andrews et al., 1987).

Figures 4a1 and 4a2 reveal, respectively, meridional and vertical components of the wave-induced eddy circulation before the composite SSW. Figure 4a2 shows that atmospheric waves produce strong upward flows at middle latitudes of the Northern Hemisphere, which enhance northward winds at high latitudes with a maximum at altitudes 40 – 50 km in Figure 4a1 and enhance downward flows near the North Pole. This is consistent with the existing theory (Andrews et al., 1987; Butchart, 2014). Areas of eddy-induced flows are produced by the SPWs propagating upward from the northern troposphere along the waveguides (e.g., Dickinson, 1968; Gavrilov et al., 2018). These waveguides expand to the summer hemisphere above the stratospheric heights, leading to SPW propagation there and production of substantial eddy velocity components in the Southern Hemisphere in Figure 4a. This eddy contribution is directed generally opposite to the Eulerian mean circulation (see Fig.3a in Koval et al., 2019a) in the stratosphere and is co-directional in the MLT region. Peak values of eddy components in Figure 4a may substantially exceed the residual components in respective atmospheric regions in Figure 3a. This reveals substantial compensation of eddy flows by the Eulerian zonal-mean circulation. However, residual meridional and vertical velocity components in Figure 3a demonstrate the main features of eddy components shown in Figure 4a, which shows that the wave-induced eddy circulation may substantially influence RMC.

In Figure 4a2 in the Northern Hemisphere, the wave-induced eddy upward vertical velocity have maxima at middle latitudes at altitudes above 20 km, which corresponds to the northward meridional velocity in Figure 4a1 at high latitudes and to

320 enhanced downward flows near the North Pole. Figure 4b2 shows that during simulated SSWs the region of strong upward eddy vertical velocities is shifted to higher northern latitudes. This shift produces negative add-ons of meridional velocity in Figure 4b1 at latitudes lower 60 - 70°N, which are generally opposite to the RMC meridional velocity in Figure 3a1. However, the latitudinal shift of eddy upward fluxes in Figure 4b2 enhances northward eddy meridional velocities near the North Pole in Figure 4b1, which form enhanced eddy downward flows at altitudes below 60 km and upward flows above 60 km near the

325 North Pole during SSW in Figure 4b2. Meridional eddy add-ons in Figure 4b1 have positive values at altitudes 60 – 70 km, which can be associated with respective region of positive add-ons of residual meridional velocity during SSW in Figure 3b1. Figure 4c2 shows that after SSW, region of maximum positive add-ons of eddy vertical velocity shifts northward to polar latitudes. It produces strong upward transport and adiabatic cooling at altitudes below 50 – 60 km, which tends to recover stratospheric temperature and stratopause height in polar region (see discussions in sections 4 and 5).

330 At the middle latitudes of the Southern Hemisphere at altitudes above 60 km one can see a region of positive add-ons of eddy vertical velocity during and after SSW in Figures 4b2 and 4c2, which becomes stronger after SSW and corresponds to respective add-ons of eddy meridional velocity in Figures 4b1 and 4c1. This may confirm that PW propagation from the northern winter stratosphere along waveguides extending to the summer hemisphere at altitudes above 60 km may modify eddy and residual circulation in the MLT region of the Southern Hemisphere. Figures 3 and 4 show differences in residual and

335 eddy meridional and vertical velocities during and after SSW compared those before the event at altitudes below 60 km. However, these differences are small and can be connected with seasonal changes in the velocity components as far as the time intervals before SSW and after SSW are separated by about three weeks.

Arrows in the bottom panels of Figure 4 represent schematic vectors of zonal-mean eddy mass fluxes calculated using Eq. (6) with replacing $\overline{v_i^* \overline{v_i}^*}$ by eddy velocity components $\overline{v_i'}, \overline{v}_{eddy}, \overline{w}_{eddy}$. These arrows visualize all peculiarities of evolution of

340 eddy circulation at different stages of the composite SSW. Contributions of the wave-induced eddy circulation lead in general to weakening of the residual mass fluxes in the northern stratosphere. Similar results were discussed by Garny et al. (2014), who showed that eddy component may cause recirculation of air in the stratosphere, and may increase the mean age-of-air, which is equivalent to deceleration of the Eulerian zonal-mean circulation by the eddy circulation.

General similarity of variations of residual and eddy velocity components and mass fluxes in Figures 3 and 4 at different stages

345 of simulated SSWs demonstrate that non-zonal global-scale wave motions can produce changes in the eddy and residual circulation. These changes are important for developing stratospheric warming events and for the transport of mass and conservative tracers in the middle and upper atmosphere.

7. ~~Conclusion~~

7. Summary

350 In the present study, estimations of the mean residual meridional circulation are performed, using temperature and wind fields obtained from a set of numerical simulations of the atmospheric general circulation with the MUAM model. The focus is made on changes of the RMC and corresponding fluxes of atmospheric mass at different stages of simulated SSW events. To achieve sufficient statistical significance, the results of numerical simulations are averaged over 19-member ensembles of the MUAM runs having SSW events. Similarities exist between the RMC simulated with the MUAM and that obtained from the MERRA-

355 2 reanalysis database, and with results of other models as well.

The changes in the RMC at altitudes of 0 – 100 km at different stages of the composite SSW event are simulated. Before SSWs in the Northern Hemisphere, the RMC with northward meridional and downward vertical velocities is dominating in the middle and upper atmosphere. Downward flows are maximum at high latitudes. During and after the composite SSW, general

deceleration of downward vertical flows at the middle northern latitudes slow-down northward RMC in the most of the analyzed altitude regions. Decreases in the residual meridional velocity at MLT heights may reach up to 30% in the Northern Hemisphere and up to 40 % in the Southern Hemisphere during and after simulated SSWs. However, situation is different at high latitudes of the Northern (winter) Hemisphere. During the composite SSW, at latitudes higher 60°N and altitudes of about 20 – 70 km, northward add-ons to the residual meridional velocity produce increased downward flows at altitudes below 45 - 50 km and upward flows at higher altitudes near the North Pole. Increased downward flows produce respective transport of heat. In addition, downward and upward flows may create adiabatic heating below 45 – 50 km altitude and adiabatic cooling above it helping downward shift of the polar stratopause during the composite SSW. After SSW, add-ons to the residual vertical velocity near the North Pole are positive at altitudes below 40 – 50 km and negative above 50 km. They produce additional cooling the stratosphere and heating the mesosphere helping to restore the height of the stratopause at polar latitudes. The wave-induced eddy circulation, which is the difference between the residual and Eulerian zonal-mean circulations, exhibits properties similar to those described above. Changes of RMC at high northern latitudes can be connected with the wave-induced zone of upward vertical flows in the stratosphere and mesosphere, which is located at latitudes 30 - 50° N before the composite SSW, at 50 - 70° N during SSW and 60 -90° N after SSW. RMC changes in the MLT region of the Southern Hemisphere may be produced by planetary waves modified by SSW and propagating from the Northern Hemisphere along waveguides, which cross the Equator at altitudes above 60 km. ~~Discussed above changes in RMC velocity components, may produce respective changes in the eddy and residual global-scale fluxes of atmospheric mass, heat and conservative aerosol and gas species, which can substantially influence thermal regime and composition of the middle and upper atmosphere.~~ Our simulations showed that changes in RMC velocity components during SSW produce respective changes in the eddy and residual global-scale fluxes of atmospheric mass and heat, which can lead to variations in concentration of conservative aerosol and gas species, and can substantially influence thermal regime and composition of the middle and upper atmosphere.

Author contribution. AK developed software packages for calculating the RMC, provided general management of the studies and formed a draft of the article. ~~AB~~AY and KD performed model simulations. TE compared the data obtained with reanalysis database. NG and AP supervised the setting of numerical experiments with the MUAM. OT participated in statistical data processing. AZ calculated and analyzed fluxes of mass. CW and KW contributed to the interpretation of mass fluxes data and revising the manuscript. All participants took part in the preparation of the final version of the article.

Acknowledgements. Developing new programs for analyzing RMC based on ensembles of with the MUAM was supported by the Russian Science Foundation (grant #20-77-10006). WC and KW are supported by National Natural Science Foundation of China (Grant No. 42011530082). Performing of numerical experiments and their analysis were supported by the Russian Foundation for Basic Research (grant #20-55-53039). In accordance with the statement 1296 of the Civil Code of the Russian Federation, the Russian State Hydrometeorological University (RSHU) has all rights on the MUAM code. To access and use the computer codes one should obtain a permission from the Rector of RSHU via the address 79, Voronezhskaya street, St. Petersburg, Russia, 192007, phone: 007 (812) 372-50-92. The authors can assist in obtaining the permission.

References

Andrews, D. G., and McIntyre, M. E.: Planetary waves in horizontal and vertical shear: The generalized Eliassen–Palm relation and the mean zonal acceleration, J. Atmos. Sci., 33, 2031–2048, 1976.

Andrews, D.G., Holton, J.R., Leovy, C.B.: Middle Atmosphere Dynamics, Academic Press, Orlando, FL. 1987.

Bal, S., Schimanke, S., Spangehl, T., and Cubasch, U.: Enhanced residual mean circulation during the evolution of split type sudden stratospheric warming in observations and model simulations, J. Earth Syst. Sci. 127:68 Indian Academy of Sciences https://doi.org/10.1007/s12040-018-0972-x, 2017.

Birner, T., Bönisch, H.: Residual circulation trajectories and transit times into the extratropical lowermost stratosphere, Atmos.

400   Chem. Phys., 11, 817—827, doi 10.5194/acp-11-817-2011, 2011.

Brewer, A. W.: Evidence for a world circulation provided by measurements of helium and water vapour distribution in the stratosphere, Q. J. R. Meteorol. Soc., 75, 351–363, doi:10.1002/qj.49707532603, 1949.

Butchart, N.: The Brewer-Dobson circulation, Rev. Geophys., 52, 157—184, doi:10.1002/2013RG000448, 2014.

de la Camara, A., Abalos, M., Hitchcock, P.: Changes in Stratospheric Transport and Mixing During Sudden Stratospheric

405   Warmings, Journal of Geophysical Research: Atmospheres 123(7), 3356–3373, doi: 10.1002/2017JD028007, 2018.

Chandran, A., Collins, R. L., Garcia, R. R., Marsh, D. R., Harvey, V. L., Yue, J., de la Torre, L..: A climatology of elevated stratopause events in the whole atmosphere community climate model, J. Geophys. Res. Atmos., 118, 1234-1246, doi:10.1002/jgrd.50123, 2013.

Charlton, A.J., Polvani, L.M.: A new look at stratospheric sudden warmings. Part I: Climatology and modelling benchmarks,

410   J. Clim. 20, 449–469, 2007.

Charney, J. G., and Drazin, P. G.: Propagation of planetary-scale disturbances from the lower into the upper atmosphere, J. Geophys. Res. 66, 83–109, 1961.

Cionni, I., Eyring, V., Lamarque, J.F. et al.: Ozone database in support of CMIP5 simulations: Results and corresponding radiative forcing, Atmos. Chem. Phys. 11. 11267–11292, doi:10.5194/acp-11-11267-2011, 2011.

415   Dickinson, R. E.: Planetary Rossby waves propagating vertically through weak westerly wave guides. J. Atmos. Sci. 25, 984−1002, 1968.

Dobson, G. M. B.: Origin and distribution of polyatomic molecules in the atmosphere, Proc. R. Soc., A236, 187–193, 1956.

Dobson, G. M. B., D. N. Harrison, and Lawrence J.: Measurements of the amount of ozone in the Earth's atmosphere and its relation to other geophysical conditions, Proc. R. Soc., A122, 456–486, 1929.

420   Eliassen, A., Palm, E.: On the transfer of energy in stationary mountain waves, Geophys. Norv. 22, 1—23, 1961.

Eluszkevicz, J., Crisp, D., Zurek, R., Elison, L. et al.: Residual circulation in the Stratosphere and lower Mesosphere as diagnosed from Microwave Limb Sounder Data, J. Atm. Sci. 53(2). 217—240, 1996.

Eyring, V., et al.: A Strategy for process-oriented validation of coupled chemistry-climate models, Bull. Am. Meteorol. Soc., 86, 1117–1133, doi:10.1175/BAMS-86-8-1117, 2005.

425   Fishman, J., Crutzen, P. J. The origin of ozone in the troposphere, Nature, 274, 855—857, 1978.

Fröhlich, K., Pogoreltsev, A., Jacobi, Ch.: Numerical simulation of tides, Rossby and Kelvin waves with the COMMA-LIM model, Advances in Space Research, 32, 863—868, 2003.

Fuller-Rowell, T., Wu, F., Akmaev, R., Fang, T.-W., Araujo-Pradere, E.: A whole atmosphere model simulation of the impact of a sudden stratospheric warming on thermosphere dynamics and electrodynamics, J. Geophys. Res., 115, A00G08, doi:

430   10.1029/2010JA015524, 2010.

Funke, B., Lopez-Puertas, M., Bermejo-Pantaleon, D., Garcia-Comas, M., Stiller, G.P., von Clarmann, T., Kiefer, M., Linden, A.: Evidence for dynamical coupling from the lower atmosphere to the thermosphere during a major stratospheric warming, Geophys. Res. Lett., 37, L13803, doi: 10.1029/2010GL043619, 2010.

Garny, H., Birner, T., Bönisch, H., and Bunzel, F.: The effects of mixing on age of air, J. Geophys. Res., 119, 7015–7034,

435   doi:10.1002/2013JD021417, 2014.

Gavrilov, N.M., Kshevetskii, S.P., Koval, A.V.: Thermal effects of nonlinear acoustic-gravity waves propagating at thermospheric temperatures matching high and low solar activity, Journal of Atmospheric and Solar-Terrestrial Physics, 208, 105381, doi 10.1016/j.jastp.2020.105381, 2020.

Gavrilov, N.M., Koval, A.V., Pogoreltsev, A.I., Savenkova, E.N.: Simulating influences of QBO phases and orographic gravity

440   wave forcing on planetary waves in the middle atmosphere, Earth Planets Space, 67(86), doi 10.1186/s40623-015-0259-2, 2015.

Gavrilov, N.M., Koval, A.V., Pogoreltsev, A.I., Savenkova, E.N.: Simulating planetary wave propagation to the upper atmosphere during stratospheric warming events at different mountain wave scenarios, Advances in Space Research, 61, 7, 1819-1836. doi 10.1016/j.asr.2017.08.022, 2018.

445 Gavrilov, N.M., Pogoreltsev, A.I., Jacobi, Ch.: Numerical modeling of the effect of latitude-inhomogeneous gravity waves on the circulation of the middle atmosphere, Izv., Atmos. Ocean. Phys., 41(1), 9–18, 2005.

Gelaro, R., McCarty, W., Suárez, M. J., Todling, R. et al.: The Modern-Era Retrospective Analysis for Research and Applications, version 2 (MERRA-2), J. Climate. 30(14)., 5419—5454, doi: 10.1175/JCLI-D-16-0758.1, 2017.

Gerber, E. P., et al.: Assessing and understanding the impact of stratospheric dynamics and variability on the earth system,
450 Bull. Am. Meteorol. Soc., 93, 845–859, doi:10.1175/BAMS-D-11-00145.1, 2012.

Gille, J. C., Lyjak, L. V., Smith, A.: The Global Residual Mean Circulation in the Middle Atmosphere for the Northern Winter Period, J. Atm. Sci., 44(10) 1437—1452, 1987.

Haynes, P.H., McIntyre, M. E., Shepherd, T. G., Marks, C. J., Shine, K. P.: On the "downward control" of extratropical diabatic circulations by eddy-induced mean zonal forces, J. Atmos. Sci. 48(4), 651−678, 1991.

455 Hassler, B., Bodeker, G.E., Dameris, M.: Technical Note: A new global database of trace gases and aerosols from multiple sources of high vertical resolution measurements, Atmos. Chem. Phys., 8, 5403–5421, 2008.

Holton, J. R.: An Introduction to Dynamic Meteorology, Fourth edition. Elsevier Academic Press., 2004.

Holton, J. R., Haynes, P. H., McIntyre, M. E., Douglas, A. R., Rood, R. B., Pfister, L.: Stratosphere-troposphere exchange, Rev. Geophys., 33, 403-439, 1995.

460 Iwasaki, T., Hamada, H., and Miyazaki, K.: Comparisons of Brewer-Dobson circulations diagnosed from reanalyses, J. Meteor. Soc. Japan, 87(6), 997–1006. doi: 10.2151/jmsj.87.997, 2009.

Jacob, D. J. Introduction to Atmospheric Chemistry, Princeton University Press, 280p, 1999.

Kobayashi, C., Iwasaki, T.: Brewer-Dobson circulation diagnosed from JRA-55, Journal of Geophysical Research 121(4), 1493-1510, 2016.

465 Kobayashi, S., Ota, Y., & Harada, H.: The JRA-55 Reanalysis: General specifications and basic characteristics, Journal of the Meteorological Society of Japan, 93, 5–48. https://doi.org/10.2151/jmsj.2015-00, 2015.

Koval, A.V., Gavrilov, N.M., Pogoreltsev, A.I., Drobashevskaya, E.A.: Numerical simulation of the mean meridional circulation in the middle atmosphere at different phases of stratospheric warmings and mountain wave scenarios, Journal of Atmospheric and Solar-Terrestrial Physics, 183, 11-18, Doi: 10.1016/j.jastp.2018.12.012, 2019a.

470 Koval, A.V., Gavrilov, N.M., Pogoreltsev, A.I., Savenkova, E.N.: Comparisons of planetary wave propagation to the upper atmosphere during stratospheric warming events at different QBO phases, J. Atmos. Solar-Terr. Phys.,171, 201—209, doi: 10.1016/j.jastp.2017.04.013, 2018.

Koval, A. V., Gavrilov, N. M., Pogoreltsev, A. I., Shevchuk, N. O.: Reactions of the middle atmosphere circulation and stationary planetary waves on the solar activity effects in the thermosphere. Journal of Geophysical Research: Space Physics,
475 124, 10645-10658 doi: 10.1029/2019JA027392, 2019b.

Laskar, F.,I., McCormack, J.P., Chau, J.L., Pallamraju, Hoffmann, D.P., Singh, R.P.: Interhemispheric Meridional Circulation During Sudden Stratospheric Warming, Journal of Geophysical Research: Space Physics, 124(8), 7112-7122, 2019.

Laštovicka, J.: Forcing of the ionosphere by waves from below, J. Atmos. Sol.-Terr. Phys., 68(3), 479–497, 2006.

Li, Q, Graf, H-F, Giorgetta, M.A.: Stationary planetary wave propagation in Northern Hemisphere winter – climatological
480 analysis of the refractive index, Atmos. Chem. Phys., 7, 183–200, 2007.

Lindzen, R. S.: Turbulence and stress owing to gravity wave and tidal breakdown, J. Geophys. Res., 86, 9707–9714, 1981.

Liu, H., Doornbos, E., Yamamoto, M., Ram, S.T.: Strong thermospheric cooling during the 2009 major stratosphere warming, Geophys. Res. Lett., 38, L12102, doi: 10.1029/2011GL047898, 2011.

McIntyre, M.E.: How well do we understand the dynamics of stratospheric warmings. J. Meterol. Soc. Japan., 60, 37-64, 1982.

485   Nath, D., Chen, W., Zelin, C., Pogoreltsev A.I., Wei, K.: Dynamics of 2013 Sudden Stratospheric Warming event and its impact on cold weather over Eurasia: Role of planetary wave reflection, Sci. Rep., 6, 24174, doi: 10.1038/srep24174, 2016.

Pawson, S., et al.: The GCM-Reality Intercomparison Project for SPARC (GRIPS): Scientific issues and initial results, Bull. Am. Meteorol. Soc., 81, 781–796, doi:10.1175/1520-0477(2000)081<0781:TGIPFS>2.3.CO;2, 2000.

Pogoreltsev, A.I., Vlasov, A.A., Froehlich, K., Jacobi, Ch.: Planetary waves in coupling the lower and upper atmosphere, J.

490   Atmos. Solar-Terr. Phys., 69, 2083–2101, doi: 10.1016/j.jastp.2007.05.014, 2007.

Pogoreltsev, A. I., Kanukhina, A. Yu., Suvorova, E. V., Savenkova, E. N.: Variability of Planetary Waves as a Signature of Possible Climatic Changes, J. Atmos. Solar-Terr. Phys., 71, 1529-1539, doi:10.1016/j.jastp.2009.05.011, 2009.

Pogoreltsev, A.I., Savenkova, E.N., Pertsev, N.N.: Sudden stratopheric warmings: the role of normal atmospheric modes, Geomagnetism and Aeronomy, 54(3), 357–372, 2014.

495   Randel, W.J., Wu, F.: A stratospheric ozone profile data set for 1979-2005: Variability, trends, and comparisons with column ozone data, J. Geophys. Res., 112, D06313, doi:10.1079/2006JD007339, 2007.

Rice, J.A.: Mathematical statistics and data analysis (3rd edition), Pacific Grove. Duxbury Press, 603 p. ISBN-10: 0534399428, 2006.

Savenkova, E.N., Gavrilov, N.M., Pogoreltsev, A.I.: On statistical irregularity of stratospheric warming occurrence during

500   northern winters, Journal of Atmospheric and Solar-Terrestrial Physics, 163, 14–22, doi: 10.1016/j.jastp.2017.06.007, 2017.

Seviour, W. J. M., N. Butchart, Hardiman, S.C.: The Brewer-Dobson circulation inferred from ERA-Interim, Q. J. R. Meteorol. Soc., 138, 878–888, doi:10.1002/qj.966, 2012.

Shepherd T. G.: Transport in the middle atmosphere, J. Meteor. Soc. Japan., 85B, 165—191, 2007.

Siskind, D.E., Eckermann, S.D., McCormack, J.P., Coy, L., Hoppel, K.W., Baker, N.L.: Case studies of the mesospheric

505   response to recent minor, major and extended stratospheric warmings, J. Geophys. Res. 115, D00N03, doi: 10.1029/2010JD014114, 2010.

Song, B-G., Chun H-Y., Residual Mean Circulation and Temperature Changes during the Evolution of Stratospheric Sudden Warming Revealed in MERRA // Atmos. Chem. Phys. Discuss., doi:10.5194/acp-2016-729, 2016

SPARC CCMVal,: SPARC report on the evaluation of chemistry-climate models, in SPARC Report No. 5, WCRP-132,

510   WMO/TD-No, edited by V. Eyring, T. G. Shepherd, and D. W. Waugh, 2010.

Stray, N. H., Orsolini, Y. J., Espy, P. J., Limpasuvan, V., Hibbins R. E.: Observations of planetary waves in the mesosphere-lower thermosphere during stratospheric warming events, Atmos. Chem. Phys., 15(9), 4997-5005, 2015.

Sun, L., Robinson, W.A.: Downward influence of stratospheric final warming events in an idealized model, Geophys. Res. Lett., 36, L03819, doi: 10.1029/2008GL036624, 2009.

515   Suvorova, E.V., Pogoreltsev, A.I.: Modeling of nonmigrating tides in the middle atmosphere, Geomagmetizm and Aeronomy. 51(1), 105-115, 2011.

Suvorova E.N., Drobashevskaya E.A., and Pogoreltsev A.I.: Climatic three-dimensional ozone distribution model based on MERRA reanalysis data, Proceedings of the Russian State Hydrometeorological University (in russian), 49, 38-46, 2017.

Swinbank, R., O'Neill, A.: Stratosphere-troposphere assimilation system, Mon. Weather Rev., 122, 686–702, 1994.

520   Swinbank R., Keil M., Jackson D., Scaife A. // United Kingdom, NWP, Met Office Bracknell, RG12 2SZ. 2004. P. 147-154

Tao, M.C., Liu, Y., Zhang, Y. L.: Variation in Brewer–Dobson circulation during three sudden stratospheric major warming events in the 2000s, Adv. Atmos. Sci., 34(12), 1415–1425, doi:10.1007/s00376-017-6321-1, 2017.

Tegtmeier, S., K. Krüger, I. Wohltmann, K. Schoellhammer, Rex, M.: Variations of the residual circulation in the Northern Hemispheric winter, J. Geophys. Res., 113, D16109, doi:10.1029/2007JD009518, 2008.

525   Yigit, E., and Medvedev, A. S.: Heating and cooling of the thermo-sphere by internal gravity waves, Geophysical Research Letters, 36, L14807, https://doi.org/10.1029/2009GL038507, 2009.

Yuan, T., Thurairajah, B., She, C.-Y., Chandran, A., Collins, R.L., Krueger, D.A.: Wind and temperature response of midlatitude mesopause region to the 2009 sudden stratospheric warming, J. Geophys. Res., 117, D09114. doi: 10.1029/2011JD017142, 2012.

530
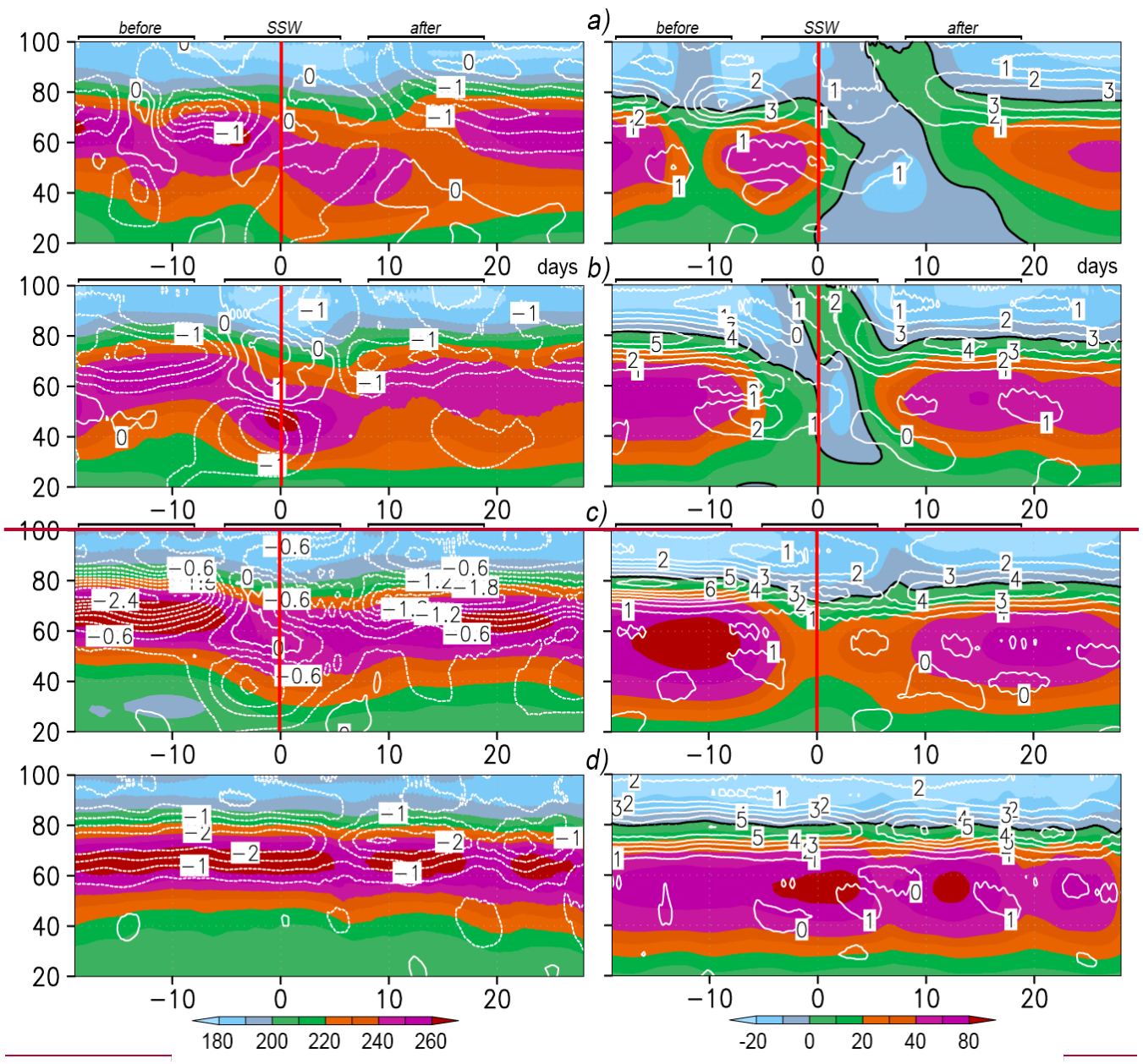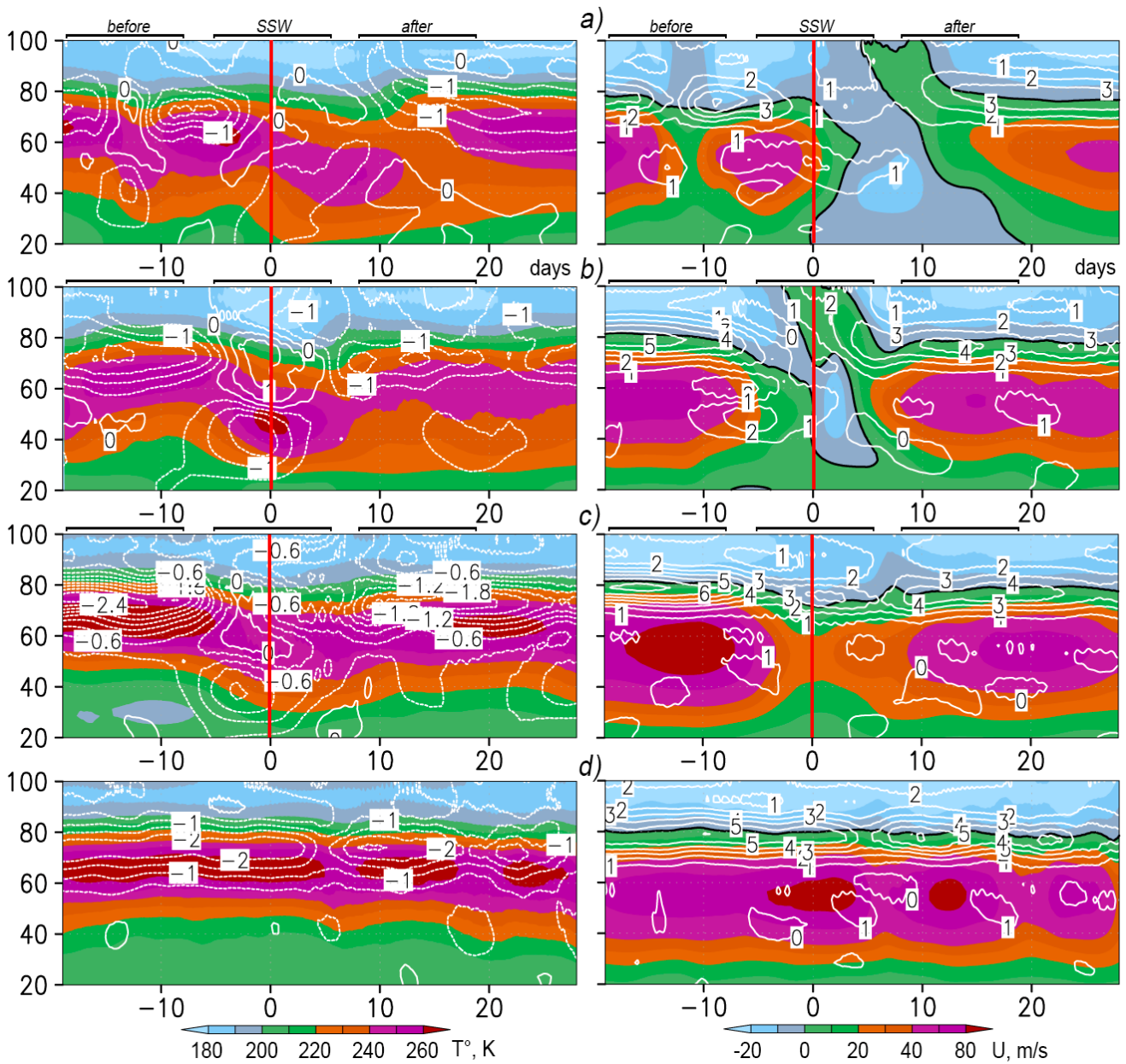
Figure 1: Examples of simulated zonal-mean temperature in K averaged over latitudinal band of 82 – 87 N (shaded left) and zonal-mean zonal wind in m/s at 62° N (shaded right) for MUAM runs with different phases of stratospheric vacillations. Panels a – d show, respectively, major SSW, HSW, minor SSW and a MUAM run without stratospheric warming. Contours show residual vertical velocity in cm/s (left) and residual meridional velocity in m/s (right) at respective latitudes (negative - dashed). Zero days correspond to the respective SSW onset dates. Horizontal lines above the plots show time intervals before, during and after SSW.

540
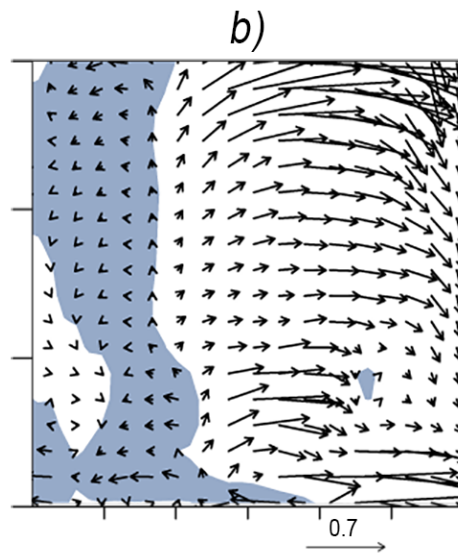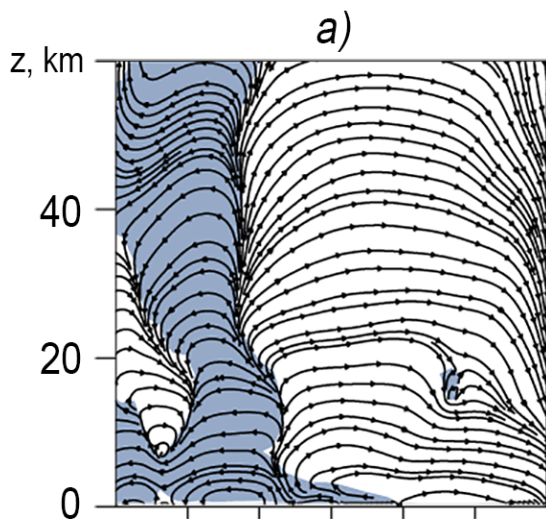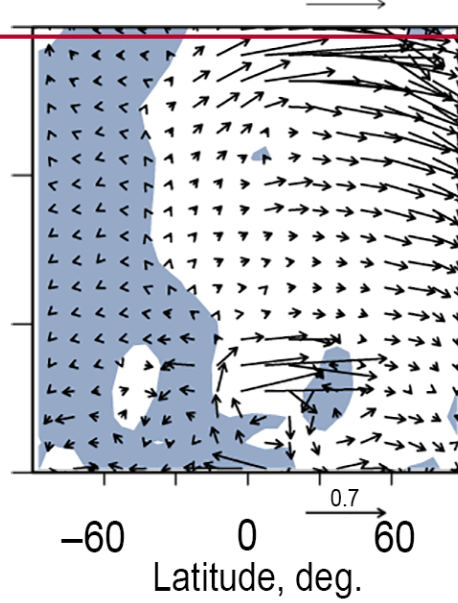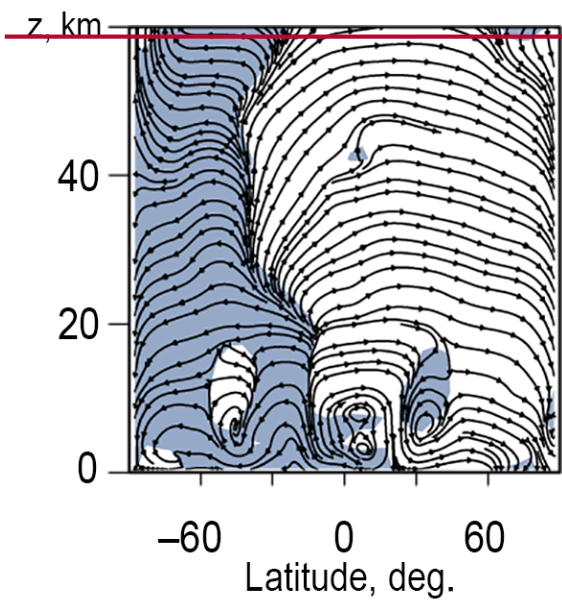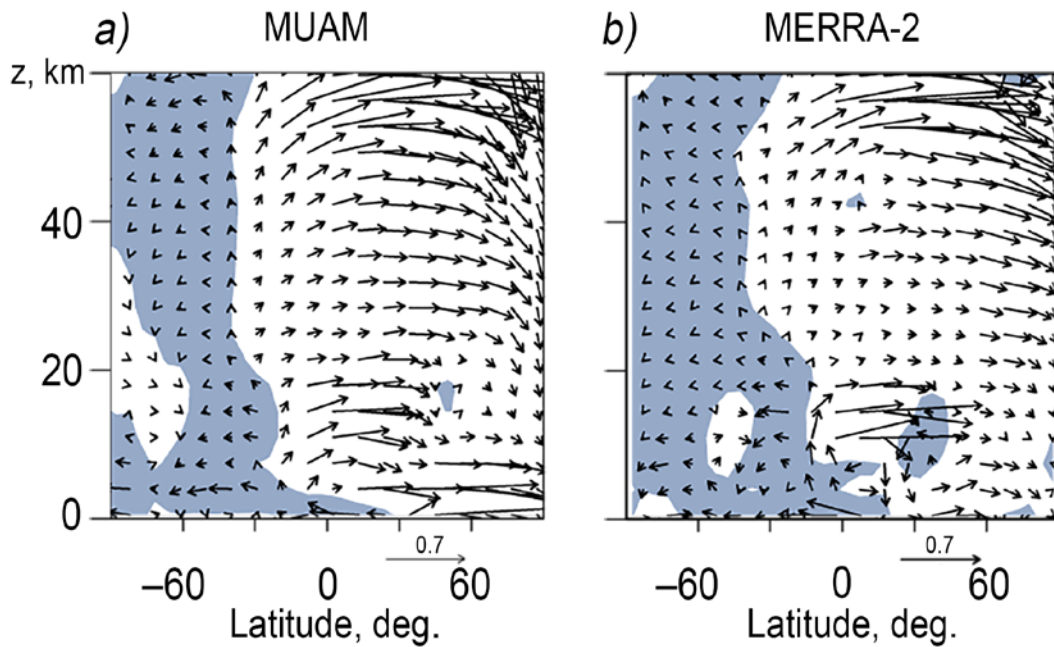
Figure 2: Latitude-altitude distributions of the RMC ~~schematic streamlines (a) and~~ wind vectors ~~(b)~~ averaged over 19 MUAM runs (~~top~~a) and according to the MERRA-2 reanalysis data (~~bottom~~b) for January. Areas with negative (southward) residual meridional wind are shaded with the gray-blue color. The ~~streamlines and~~ vectors are shown for the vertical velocity multiplied by factor 100.
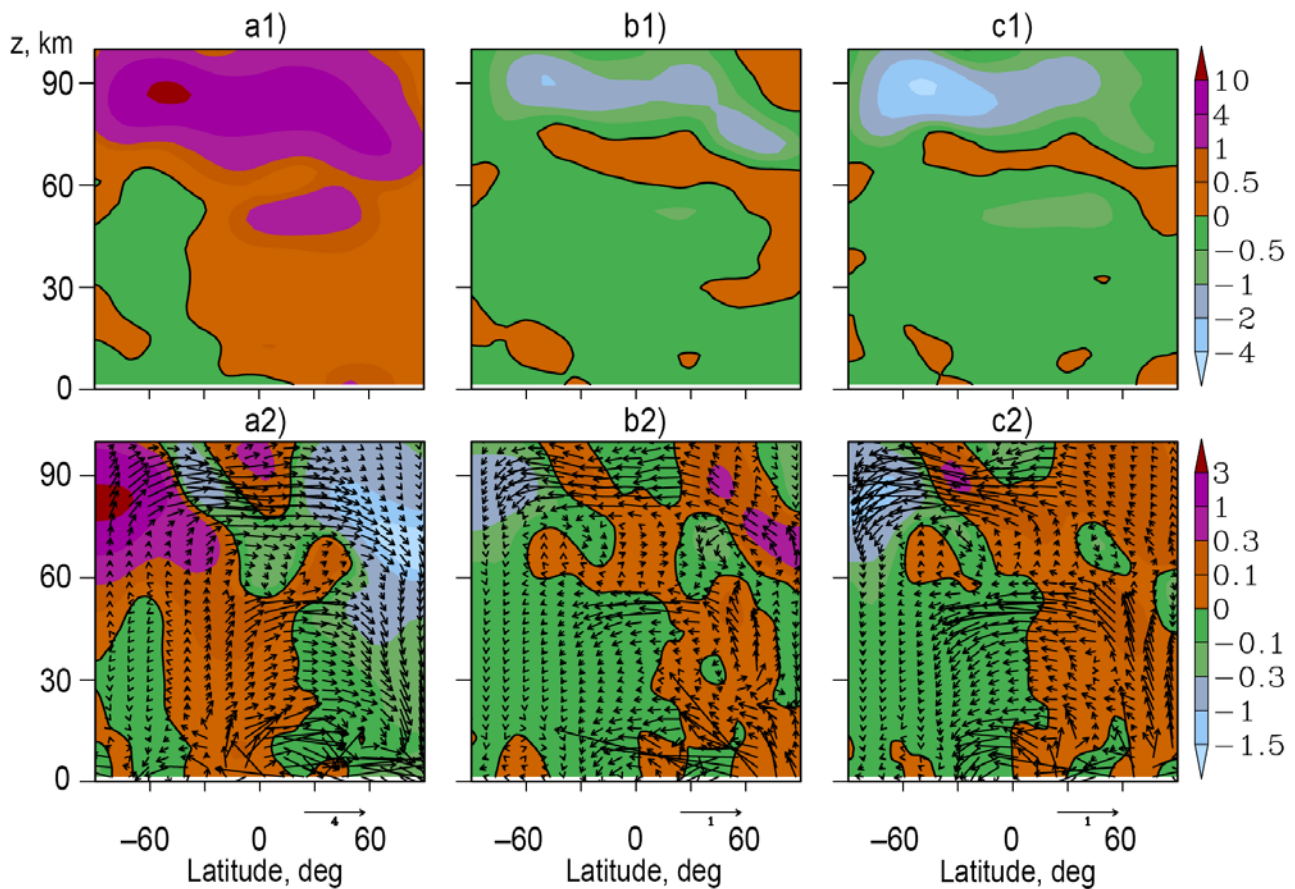
Figure 3: Zonal-mean residual meridional velocity in m/s (a1) and vertical velocity in cm/s (a2) averaged over 19 MUAM runs for 11-day intervals before the composite SSW and add-ons of respective quantities at the time intervals during SSW (b) and after SSW (c). Arrows show vectors with components $r \cdot F_x^*$ and $100 \cdot r \cdot F_z^*$ in kg·m^{-2}s^{-1}, which schematically

represent zonal-mean RMC mass fluxes and their respective add-ons, where $r = 10exp(z/15)$ is a scale factor used for better schematic representation at high altitudes. Solid contours correspond to zero values. All SSW events are observed in January – February.
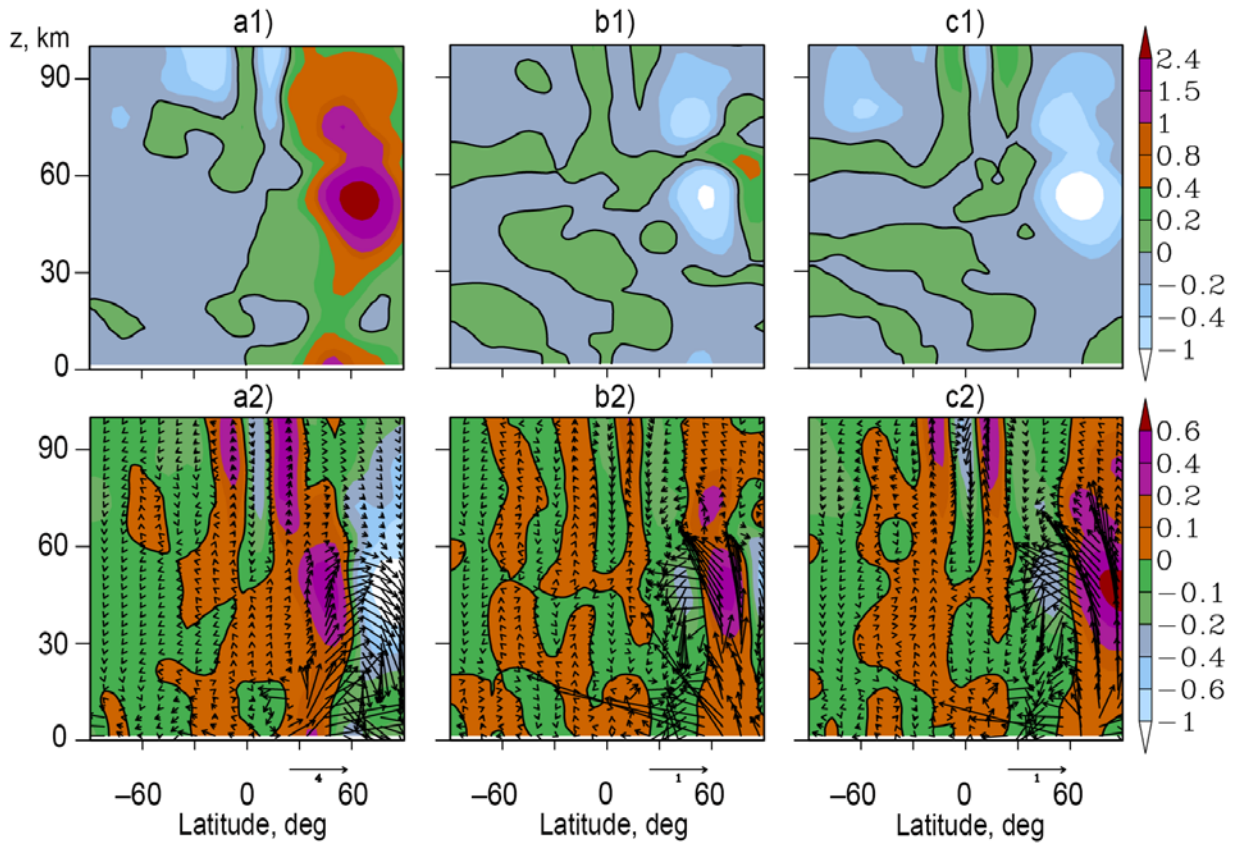
Figure 4: The same as Fig. 3 but for the meridional and vertical components of the wave-induced eddy circulation.